CORA Cork Open Research Archive
Cartlann Taighde Oscailte Chorcaí

Title	Orthogonal chirp division multiplexing for coherent optical fiber communications
Authors	Ouyang, Xing;Zhao, Jian
Publication date	2016-08-07
Original Citation	Ouyang, X. and Zhao, J. (2016). Orthogonal chirp division multiplexing for coherent optical fiber communications. Journal of Lightwave Technology, 34, 4376-4386. doi: 10.1109/JLT.2016.2598575
Type of publication	Article (peer-reviewed)
Link to publisher's version	10.1109/JLT.2016.2598575
Rights	© 2016 IEEE. Personal use of this material is permitted. Permission from IEEE must be obtained for all other uses, in any current or future media, including reprinting/republishing this material for advertising or promotional purposes, creating new collective works, for resale or redistribution to servers or lists, or reuse of any copyrighted component of this work in other works.
Download date	2026-09-08 04:01:10
Item downloaded from	https://hdl.handle.net/10468/3217

UCC
University College Cork, Ireland
Coláiste na hOllscoile Corcaigh

Orthogonal Chirp Division Multiplexing for Coherent Optical Fiber Communications

Xing Ouyang and Jian Zhao

***Abstract*—In this paper, we propose an orthogonal chirp division multiplexing (OCDM) technique for coherent optical communication. OCDM is the principle of orthogonally multiplexing a group of linear chirped waveforms for high-speed data communication, achieving the maximum spectral efficiency (SE) for chirp spread spectrum, in a similar way as the orthogonal frequency division multiplexing (OFDM) does for frequency division multiplexing. In the coherent optical (CO)-OCDM, Fresnel transform formulates the synthesis of the orthogonal chirps; discrete Fresnel transform (DFnT) realizes the CO-OCDM in the digital domain. As both the Fresnel and Fourier transforms are trigonometric transforms, the CO-OCDM can be easily integrated into the existing CO-OFDM systems. Analyses and numerical results are provided to investigate the transmission of CO-OCDM signals over optical fibers. Moreover, experiments of 36-Gbit/s CO-OCDM signal are carried out to validate the feasibility and confirm the analyses. It is shown that the CO-OCDM can effectively compensate the dispersion and is more resilient to fading and noise impairment than OFDM.**

***Index Terms*—Chirp spread spectrum, coherent optical communication, discrete Fresnel transform, Fresnel diffraction integral, orthogonal chirp division multiplexing (OCDM), orthogonal frequency division multiplexing.**

I. Introduction

BY virtue of the recent advances in optical communication technologies, the capacity of fiber-optic systems is multiplied over the last few decades. Optical coherent detection and high-speed CMOS are two of the crucial technologies contributing to the advances, as they enable sophisticated digital signal processing (DSP) technologies in the fiber-optic systems [1]–[3]. One of the remarkable rewards promised by DSP is that the advanced modulation and detection schemes [4]–[6], which have been widely deployed for electronic communication systems, are being migrated into fiber-optic systems, achieving higher spectral efficiency (SE) and capacity [7]–[9].

Orthogonal frequency division multiplexing (OFDM) is one of the most attractive technologies enabled by DSP for optical communications [10]–[12]. In the OFDM systems, a large group of orthogonal subcarriers are modulated and multiplexed for high-speed data communication. It attains the maximum SE of frequency division multiplexing (FDM) systems, avoiding the guard band between subcarriers in the sense of orthogonality. On the other hand, OFDM inherits the advantages promised by FDM; by conveying information in narrowband subchannels, it is resilient to channel dispersion, which can be compensated by simple single-tap equalizers.

In this paper, we propose an orthogonal chirp division multiplexing (OCDM) technique for coherent optical (CO) communications. Conventionally, chirped waveforms are of spectrum spreading scheme, or namely chirp spread spectrum (CSS) for secure and robust applications, such as military and underwater communications. In the CSS, SE is sacrificed for high processing gain and multipath resolution. OCDM in essence is the principle of synthesizing a large group of orthogonal chirps, achieving the maximum SE of the CSS systems, in a similar way as OFDM does for the FDM. Meanwhile, OCDM inherits the versatilities and advantages of CSS, e.g., resilience to the impairments due to channel fading and noise effects [13].

In the CO-OCDM system, Fresnel transform formulates the multiplexing/demultiplexing of the linear chirps, and discrete Fresnel transform (DFnT) implements the system in the digital domain [14]. More specifically, the inverse DFnT (IDFnT) generates OCDM signal at the transmitter; the DFnT recovers the OCDM signal at the receiver. According to the convolution property of the Fresnel transform, we formulate the transmission model of CO-OCDM signal to study the impairments in optical fibers. According to the eigen-decomposition of DFnT, an efficient single-tap equalizer algorithm is proposed to simplify the DSP complexity of the CO-OCDM system.

In this paper, analyses and simulations are provided to investigate the performance of the CO-OCDM system over fiber transmission. It is shown that the CO-OCDM can effectively compensate the chromatic dispersion, as the CO-OFDM does. Meanwhile, the CO-OCDM is more resilient against the fading and noise impairments in the optical fiber than the CO-OFDM. Experiments were carried out to implement transmission of 36-Gbit/s CO-OCDM signal over 80-km standard single-mode fiber (SMF) to validate the advantages of CO-OCDM system.

The OCDM inherits the robustness of CSS against the severe fading effect and noise impairment in the wireless channel. We will show that the proposed CO-OCDM system also promises the resilience against the detrimental effects in the fiber-optic channel. Moreover, by utilizing the relation between the Fresnel transform and the Fourier transform, the CO-OCDM system can be easily integrated into the widespread CO-OFDM systems with only minor modifications.

This paper is organized as follows. In Section II, we firstly have a brief review of OFDM, and then introduce the principle

Manuscript received April 9, 2016; revised June 24, 2016; accepted July 29, 2016. Date of publication August 7, 2016; date of current version September 6, 2016. This work was supported by the Science Foundation Ireland under Grant 11/SIRG/I2124 and Grant 15/CDA/3652.

X. Ouyang is with the Tyndall National Institute, Cork, Ireland, and also with the School of Electrical and Electronic Engineering, University College Cork, Cork, Ireland (e-mail: xing.ouyang@tyndall.ie).

J. Zhao is with the Tyndall National Institute, Cork, Ireland (e-mail: jian.zhao@tyndall.ie).

Digital Object Identifier 10.1109/JLT.2016.2598575

of OCDM. Their similarities and differences are discussed to show the compatibility of the OCDM to the OFDM. Section III illustrates the CO-OCDM system and formulates its transmission model over SMF channel. Transmission impairments in the fibers are analyzed, and an efficient single-tap equalization algorithm is proposed. In Section IV, analyses and simulations are provided to validate the feasibility of the CO-OCDM system, and to investigate its performance. In Section V, experimental results of a 36 Gbit/s CO-OCDM signal are presented. Finally, conclusion is provided in Section VI.

Notations: Matrices are in bold normal upper case letter, and vectors in bold italic lower case. Some notations are below.

j	$\sqrt{-1}$
$H(m, n)$	the (m, n)-th entry of matrix $\mathbf{H}$
$h(n)$	the n-th entry of vector $\boldsymbol{h}$
$(\cdot)^*$	complex conjugate operator
$(\cdot)^{\mathrm{T}}$	matrix transpose operator
$(\cdot)^{\mathrm{H}}$	complex conjugate transpose operator
$\delta(n)$	Kronecker delta function

II. Preliminaries

In this section, we firstly introduce the Fresnel integral transformation and its discrete form, discrete Fresnel transform. After that, we present the conventional OFDM and CSS systems, followed by the proposed OCDM, the approach achieving the maximum SE for CSS, as the OFDM does for FDM.

A. Fresnel Transform and Discrete Fresnel Transform

Fresnel integral transformation originates from classical optics [15]–[18]. It is the formula that mathematically describes the near-field optical diffraction. If a monochromatic plain wave with wavelength λ encounters a slit (grating) whose scale is comparable in size to λ, the diffraction pattern projected on a plate at distance z is given by

$$\hat{s}(\tau) = \mathscr{F}_a\{s(t)\}(\tau) = \frac{e^{-j\frac{\pi}{4}}}{\sqrt{a}} \int s(t)\, e^{j\frac{\pi}{a}(\tau-t)^2}\, \mathrm{d}t, \quad (1)$$

where $\mathscr{F}_a(\cdot)$ denotes the Fresnel transform. The parameter $a = \lambda z$ is the normalized Talbot distance, and $s(t)$ is the complex transmittance of the grating.

Based on [Theory (1), 19], the Fresnel transform of a linear convolution is

$$\begin{aligned} \hat{r}(\tau) &= \mathscr{F}_a\{h(t) * s(t)\}(\tau) \\ &= \hat{h}(\tau) * s(\tau) = h(\tau) * \hat{s}(\tau). \end{aligned} \quad (2)$$

Eq. (2) states that the Fresnel transform of a convolution equals either one convolving with the Fresnel transform of the other. It is different from the convolution theorem of the Fourier transform which says that the Fourier transform of a convolution equals the product of the Fourier transforms.

B. Discrete Fresnel Transform

The discrete form of Fresnel transform, DFnT relates to the Talbot effect, the periodic grating of Fresnel diffraction [15]–[18] as shown in Fig. 1. The DFnT matrix gives the field

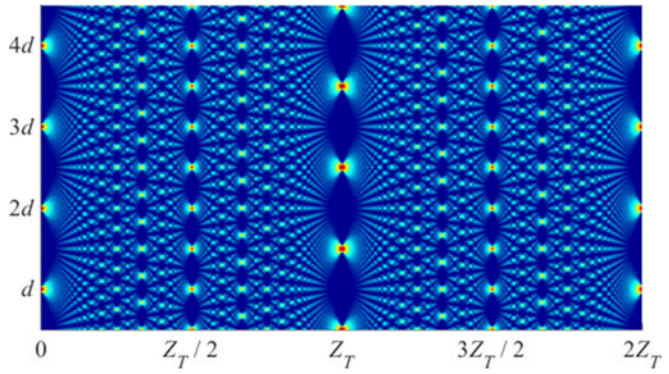

Fig. 1. Illustration of Talbot effects; the DFnT matrix of size N represents the optical field of the light spots at the fraction of Talbot distance Z_T / N.

coefficients of the Talbot image, also called the self-image, at the fraction of Talbot distance, $z = Z_T/N$, where

$$Z_T = d^2/\lambda \quad (3)$$

is the Talbot distance and d is the distance of repeated gratings.

In previous works, the DFnT is formulated for describing the coefficients of Talbot image [20]–[24]. Degeneracy exists in the DFnT matrices: the size of DFnT matrices is $N/2$ if $N \equiv 0$ and 2 (mod 4), while the size of DFnT matrices is N if $N \equiv 1$ and 3 (mod 4). The degeneracy hinders the application of DFnT as a general mathematical tool. In recent work, the DFnT is derived in [14] without such degeneracy. The (m, n)-th entry of the N by N DFnT matrix Φ is defined as

$$\Phi(m,n) = \frac{1}{\sqrt{N}} e^{-j\frac{\pi}{4}} \times \begin{cases} e^{j\frac{\pi}{N}(m-n)^2} & N \equiv 0\,(\mathrm{mod}2) \\ e^{j\frac{\pi}{N}\left(m+\frac{1}{2}-n\right)^2} & N \equiv 1\,(\mathrm{mod}2) \end{cases}. \quad (4)$$

The DFnT matrix is unitary, and its other important properties, such as its eigen-decomposition, can be found in [14]. It should be noted that the DFnT of even and odd N is slightly different.

The DFnT possesses the circular convolution property which says that the DFnT of the circular convolution of two sequences equals either one convolving with the DFnT of the other. Given two length-N vectors $\boldsymbol{h}$ and $\boldsymbol{s}$ and two N by N circulant matrices $\mathbf{H}$ and $\mathbf{S}$ whose first columns are respectively $\boldsymbol{h}$ and $\boldsymbol{s}$, the circular convolution in matrix form is

$$r = \mathbf{H}s = \mathbf{S}h. \quad (5)$$

The DFnT of the circular convolution is

$$\hat{r} = \mathbf{\Phi} r = \mathbf{H}\hat{s} = \mathbf{S}\hat{h}, \quad (6)$$

where $\hat{\boldsymbol{s}}$ and $\hat{\boldsymbol{h}}$ are the DFnTs of $\boldsymbol{s}$ and $\boldsymbol{h}$, respectively. It can be observed that the DFnT of a circular convolution in (6) is the discrete analogy of (2).

In (4), the entries of the DFnT matrices consists of that of the DFT matrix with the additional quadratic phases, as

$$\Theta_1(m) = e^{-j\frac{\pi}{4}} \times \begin{cases} e^{j\frac{\pi}{N}m^2} & N \equiv 0\,(\mathrm{mod}2) \\ e^{j\frac{\pi}{4N}} e^{j\frac{\pi}{N}\left(m^2+m\right)} & N \equiv 1\,(\mathrm{mod}2) \end{cases}, \quad (7)$$

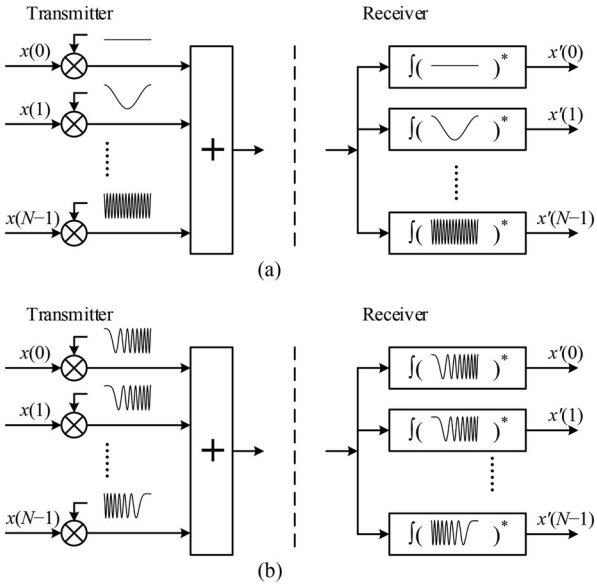

Fig. 2. Schematic diagrams of the transceivers of (a) OFDM and (b) OCDM. $x(n)$ and $x'(n)$ are transmitted and received symbols. The waveforms illustrate the (a) harmonics in OFDM and the (b) orthogonal chirps in OCDM.

and

$$\Theta_2(n) = \begin{cases} e^{j\frac{\pi}{N}n^2} & N \equiv 0 \,(\mathrm{mod}2) \\ e^{j\frac{\pi}{N}(n^2-n)} & N \equiv 1 \,(\mathrm{mod}2) \end{cases}, \tag{8}$$

Thus, the DFnT can be implemented by FFT in three steps:
1) multiplying the chirped phase Θ_1,
2) performing the DFT by the FFT algorithm, and finally
3) multiplying the other chirped phase Θ_2,

where $\boldsymbol{\Theta}_1$ and $\boldsymbol{\Theta}_2$ are diagonal matrices whose m-th diagonal entries are $\Theta_1(\mathrm{m})$ and $\Theta_2(\mathrm{m})$, respectively.

C. Orthogonal Frequency Division Multiplexing

It is well known that, prior to OFDM, FDM divides the entire bandwidth into spectrally separated subchannels. Guard bands are inserted between the subchannels to avoid inter-subcarrier interference, but resulting in the loss of SE.

Under certain *conditions* in which the frequency spacing of the subcarriers Δf is the reciprocal of the symbol period T, i.e., $\Delta f = 1/T$, the guard bands can be avoided. Although the spectra of subcarriers overlap each other, it is possible to recover the information on distinct subcarriers without any interference.

The transceiver of OFDM system is illustrated in Fig. 2(a). The Fourier transform generates the continuous time-domain OFDM signal consisting of N subcarriers,

$$s(t) = \frac{1}{\sqrt{T}} \sum_{k=0}^{N-1} x(k)\, e^{j2\pi k\Delta f \cdot t}, \tag{9}$$

where $0 \le t < T, \Delta f = 1/T$, and $x(k)$ is the symbol on the k-th subcarrier. At the receiver, the output of the matched-filter

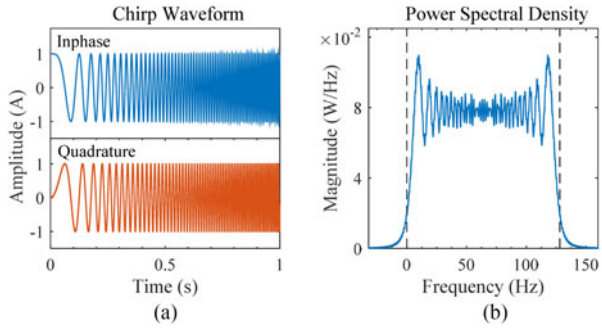

Fig. 3. Illustrations of (a) a linear chirp with a chirp rate $\alpha = 128$ and duration $T = 1$ s, and (b) its power spectrum density.

with respect to the m-th subcarrier is

$$\begin{aligned} x'(m) &= \frac{1}{\sqrt{T}} \int_0^T s(t)\, e^{-j2\pi m\Delta f \cdot t} \mathrm{d}t \\ &= \sum_{k=0}^{N-1} x(k)\, \delta(m-k) = x(m). \end{aligned} \tag{10}$$

OFDM can be realized in the digital domain by DFT [25]. At the transmitter, the discrete time-domain OFDM signal is generated by the inverse DFT (IDFT) as

$$s(n) = s(t)\Big|_{t=n\frac{T}{N}} = \frac{1}{\sqrt{N}} \sum_{k=0}^{N-1} x(k)\, e^{j\frac{2\pi}{N}kn}, \tag{11}$$

where $n = 0, 1, \ldots, N-1$. If the OFDM signal in (11) is received without any distortion, the m-th symbol is recovered by DFT at the receiver as

$$x'(m) = \frac{1}{\sqrt{N}} \sum_{n=0}^{N-1} s(n)\, e^{-j\frac{2\pi}{N}mn} = x(m). \tag{12}$$

D. Chirp Spread Spectrum

CSS has long been considered for radar and communication systems. It guarantees secure and robust communications for specific purposes, including military and underwater communications [26]–[28]. One commercial example is the CSS scheme in the 802.15a standard for ultra-wideband communication.

In the CSS, a linear chirp is the linearly frequency-modulated signal with constant amplitude,

$$\psi(t) = e^{j\left(\alpha\pi t^2 + 2\pi\beta t + \phi_0\right)}, \tag{13}$$

where α is called the chirp rate, β the carrier frequency, and φ_0 is the initial phase. In Fig. 3, a chirp with $\alpha = 128$ and a period of 1 second, as well as its spectrum, is shown. The bandwidth of a chirp is proportional to its chirp rate α; the time-bandwidth product $B \times T$ indicates its processing gain.

In the CSS system, if there exist more than one chirp in the same bandwidth and period, inter-chirp interference (ICI) occurs. Since the time-bandwidth product $B \times T >> 1$, we have $B >> R_s$, where $R_s = 1/T$ is the symbol rate. The higher the processing gain is, the lower the SE becomes. Consequently,

chirp is preferred in low data rate communications in which reliability is the priority.

E. Principle of Orthogonal Chirp Division Multiplexing

The proposed OCDM achieves the maximum SE for CSS in the sense of orthogonality. Under the *conditions* that the chirp rate $\alpha = -(N/T^2)$ and that each chirp is shifted with an integer multiple of $\Delta c = T/N$, it is able to synthesize a bank of *N* orthogonal and linear chirps without any ICI. The *k*-th chirp, for $k = 0, 1, \ldots, N-1$, is thus defined as

$$\psi_k(t) = \frac{1}{\sqrt{T}} e^{j\frac{\pi}{4}} e^{-j\pi\frac{N}{T^2}\left(t-k\frac{T}{N}\right)^2}, \tag{14}$$

where $0 \le t < T$, and one can have the property that

$$\int \psi_m^*(t)\,\psi_k(t)\,\mathrm{d}t = \delta(m-k). \tag{15}$$

Fig. 2(b) shows the chirps of a OCDM signal. The baseband ($\beta = 0$) time-domain OCDM signal is

$$s(t) = \sum_{k=0}^{N-1} x(k)\,\psi_k(t), \quad 0 \le t < T, \tag{16}$$

which can be realized by Fresnel transform. At the receiver, the symbol on the *m*-th chirp can be recovered by its matched-filter

$$\begin{aligned} x'(m) &= \int_0^T \psi_m^*(t)\,s(t)\,\mathrm{d}t \\ &= \sum_{k=0}^{N-1} x(k)\,\delta(m-k) = x(m). \end{aligned} \tag{17}$$

OCDM can be realized in the digital domain by DFnT [14]. At the transmitter, the discrete time-domain OCDM signal is obtained by IDFnT as

$$\begin{aligned} s(n) &= \frac{1}{\sqrt{N}} e^{j\frac{\pi}{4}} \sum_{k=0}^{N-1} x(k) \\ &\quad \times \begin{cases} e^{-j\frac{\pi}{N}(n-k)^2} & N \equiv 0 \,(\mathrm{mod}2) \\ e^{-j\frac{\pi}{N}\left(n-k+\frac{1}{2}\right)^2} & N \equiv 1 \,(\mathrm{mod}2) \end{cases}. \end{aligned} \tag{18}$$

If the signal in (18) is received directly at the receiver, the inverse operation recovers the symbols by performing DFnT as

$$\begin{aligned} x'(m) &= \frac{1}{\sqrt{N}} e^{-j\frac{\pi}{4}} \sum_{n=0}^{N-1} s(n) \\ &\quad \times \begin{cases} e^{j\frac{\pi}{N}(m-n)^2} & N \equiv 0 \,(\mathrm{mod}2) \\ e^{j\frac{\pi}{N}\left(m-n+\frac{1}{2}\right)^2} & N \equiv 1 \,(\mathrm{mod}2) \end{cases} \\ &= \sum_{k=0}^{N-1} x(k)\,\delta(m-k) = x(m). \end{aligned} \tag{19}$$

It is observed that the transformation pair in (18) and (19) implement the multiplexing and demultiplexing of the OCDM signal, respectively. Referring to Section II-B, they are exactly the IDFnT and DFnT.

III. OCDM for Coherent Optical Communications

In this section, we introduce the OCDM for coherent optical fiber systems. The mathematic model of the CO-OCDM signal in SMF is formulated to show the effects of linear impairments. An efficient receiver scheme is presented to compensate linear dispersion based on the eigen-decomposition of DFnT.

In Fig. 4, the schematic diagram of the CO-OCDM system is illustrated. At the transmitter, the generated CO-OCDM signal is given in (18), which is rewritten here in the matrix form

$$s = \mathbf{\Phi}^H x, \tag{20}$$

where $\boldsymbol{s} = [s(0), s(1), \ldots, s(N-1)]^T$ is the time-domain OCDM sample vector and $\boldsymbol{x} = [x(0), x(1), \ldots, x(N-1)]^T$ is the symbol vector, and Φ is the $N \times N$ DFnT matrix with its (n, k)-th entry to be $\Phi(n, k)$ in (19). The IDFnT is realized by the three-step operation involving IDFT, as in Section II-B. Guard interval is inserted between adjacent OCDM symbols. In this paper, GI is filled with cyclic prefix (CP), which is a portion of the end of the OCDM samples, as illustrated in the inset (i) in Fig. 4. After parallel-to-serial (P/S) and digital-to-analog (D/A) conversion, the output analog electrical signal is amplified to drive an optical modulator for optical transmission.

Once the modulated optical signal is fed into optical fiber for transmission, it will experience detrimental effects, such as the chromatic dispersion (CD) and polarization-mode dispersion in optical fibers, and the spontaneous amplified emission (ASE) noise introduced by optical amplifiers. The optical amplifier is usually followed by optical band-pass filter (OBPF) to remove the out-of-band ASE noise.

At the receiver end, an optical coherent receiver converts the optical signal to electrical baseband signal. The baseband signal is then sampled by analogy-to-digital (A/D) converters. If the period of guard interval (GI) is larger than the maximal delay spread of dispersion, the received CO-OCDM signal is

$$r = \mathbf{H}s + n = \mathbf{H}\mathbf{\Phi}^H x + n, \tag{21}$$

where $\mathbf{H}$ is the channel impulse response (CIR) matrix, $\boldsymbol{n}$ is the additive white Gaussian noise (AWGN) vector.

In Eq. (21), the CIR matrix $\mathbf{H}$ is an $N \times N$ circulant matrix with its first column to be $\boldsymbol{h} = [h(0), \ldots, h(L-1), 0, \ldots, 0]^T$, where $h(l), l = 0, 1, \ldots, L-1$, are the coefficients of CIR taps and L is the maximum delay spread of the dispersion. Based on the channel modelling [29], the CIR matrix $\mathbf{H}$ mathematically represents various linear filtering (bandwidth limitation) effects of electronic/optical components, such as filters, drivers, modulators and photodiodes in a communication system. It can also represent the dispersion effects in optical fiber channels, such as chromatic dispersion and polarization mode dispersion. The AWGN vector $\boldsymbol{n}$ models the additive noise in an optical system, such as the ASE noise from optical amplifiers and the thermal noise induced by photodiodes (PD).

In the following, we will introduce two receiver schemes, as shown in Fig. 4. In the receiver #1, the received signal is first operated by DFnT. Based on the circular convolution property of DFnT [14], either a (a) time-domain equalizer (TDE) or a (b) frequency domain equalizer (FDE) can compensate dispersion

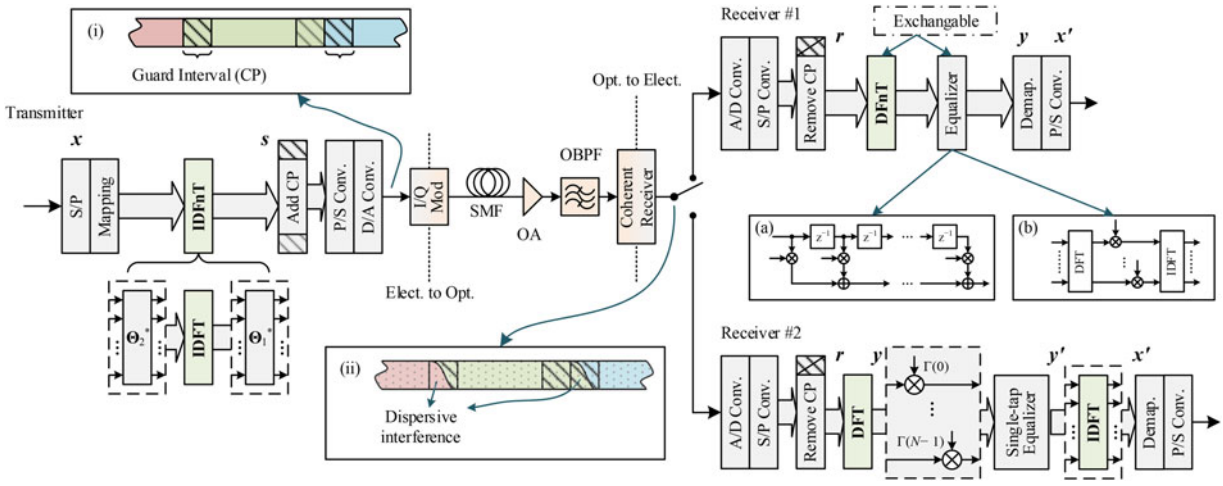

Fig. 4. Schematic diagram of the CO-OCDM system. Excluding the components in the dashed boxes, the transmitter and receiver #2 form the diagram of a conventional CO-OFDM system. Insets: illustrations of the (i) transmitted OCDM signal and the (ii) received OCDM signal distorted by dispersion and noise; (a) time-domain and (b) frequency-domain equalizers in the receiver #1.

after the DFnT. The receiver #2 is based on single-tap equalizer by utilizing the eigen-decomposition property of the DFnT. We will show that receiver #2 is more computationally efficient.

A. Receiver #1

Based on (21), the channel can be compensated before DFnT at the receiver. Once the channel is compensated, the receiver can perform DFnT, according to (19), to recover the transmitted symbols without inter-chirp interference.

Alternatively, the received signal can be first transformed by DFnT. Based on the convolution property of DFnT [14],

$$\begin{aligned} y &= \boldsymbol{\Phi} r = \boldsymbol{\Phi}\mathbf{H}\boldsymbol{\Phi}^H x + \boldsymbol{\Phi} n, \\ &= \mathbf{H} x + v, \end{aligned} \tag{22}$$

where $\boldsymbol{v} = \boldsymbol{\Phi} n$ is still AWGN as $\boldsymbol{\Phi}$ is a unitary matrix.

In Eq. (22), it can be observed that the chirp waveforms $\boldsymbol{\Phi}^H$ disappear, and the symbols $\boldsymbol{x}$ are distorted by the dispersion $\mathbf{H}$ and corrupted by the additive noise $\boldsymbol{v}$. The dispersion $\mathbf{H}$ can be compensated by either (a) TDE or (b) FDE as shown in Fig. 4. If the TDE is adopted, the received signal $\boldsymbol{y}$ is compensated by a transversal filter, in which the number of taps should be larger than the maximum excess delay spread. If FDE is adopted, the received signal is first transformed to the frequency domain by DFT. After the channel dispersion is compensated by single-tap equalizer, the frequency domain signal is transformed back to the time domain by IDFT for data recovery. In the receiver #1, if the channel dispersion is severe, FDE is preferable than TDE for its lower computational complexity.

B. Receiver #2

Another more efficient receiver scheme is presented. In the receiver #2, the received signal $\boldsymbol{r}$ is first transformed by DFT Ω, rather than the DFnT Φ, where Ω is the DFT matrix. With the substitution, $\mathbf{I} = \boldsymbol{\Omega}^H \boldsymbol{\Omega}$, where $\mathbf{I}$ is the identity matrix, one has the frequency-domain signal as

$$\begin{aligned} y &= \boldsymbol{\Omega} r = \boldsymbol{\Omega}\mathbf{H}\boldsymbol{\Phi}^H x + \boldsymbol{\Omega} n \\ &= \boldsymbol{\Omega}\mathbf{H}\boldsymbol{\Omega}^H \boldsymbol{\Omega}\boldsymbol{\Phi}^H \boldsymbol{\Omega}^H \boldsymbol{\Omega} x + w \\ &= \boldsymbol{\Lambda}\boldsymbol{\Gamma}^H \boldsymbol{\Omega} x + w, \end{aligned} \tag{23}$$

where Ω is the DFT matrix in (12), $\boldsymbol{\Lambda} = \boldsymbol{\Omega}\mathbf{H}\boldsymbol{\Omega}^H$ is the channel frequency response (CFR) matrix, $\boldsymbol{\Gamma}^H = \boldsymbol{\Omega}\boldsymbol{\Phi}^H \boldsymbol{\Omega}^H$ is a coefficient matrix, and $\boldsymbol{w} = \boldsymbol{\Omega} n$ is the noise vector. It should be noted that $\boldsymbol{w}$ is also AWGN as Ω is also unitary.

As $\mathbf{H}$ is a circulant matrix, Λ is a diagonal matrix with its k-th diagonal entry to be the CFR coefficient (or eigenvalue) of the k-th frequency bin (or the k-th column of $\boldsymbol{\Omega}^H$). Moreover, the DFnT is also a circulant matrix. Consequently, Γ is also a diagonal matrix with its diagonal entries to be the eigenvalue of Φ with respect to the IDFT matrix $\boldsymbol{\Omega}^H$. Based on [14], the k-th diagonal entry of Γ is

$$\Gamma(k) = \begin{cases} e^{-j\frac{\pi}{N}k^2} & N \equiv 0 \,(\mathrm{mod} 2) \\ e^{-j\frac{\pi}{N}k(k-1)} & N \equiv 1 \,(\mathrm{mod} 2) \end{cases}. \tag{24}$$

The CFR Λ and phase Γ^H can be compensated together as

$$\begin{aligned} y' &= \mathbf{G}\boldsymbol{\Gamma} y \\ &= \mathbf{G}\boldsymbol{\Lambda}\boldsymbol{\Omega} x + \mathbf{G}\boldsymbol{\Gamma} w, \end{aligned} \tag{25}$$

where $\mathbf{G}$ is a diagonal matrix with its k-th diagonal entry $G(k)$ to be the coefficient of the single-tap equalizer. Finally, the signal is transformed by IDFT to recover the transmitted symbols as

$$\begin{aligned} x' &= \boldsymbol{\Omega}^H y' \\ &= \boldsymbol{\Omega}^H \mathbf{G}\boldsymbol{\Lambda}\boldsymbol{\Omega} x + \boldsymbol{\Omega}^H \mathbf{G}\boldsymbol{\Gamma} w. \end{aligned} \tag{26}$$

For example, if a ZF equalizer is adopted, namely $\mathbf{G} = \boldsymbol{\Lambda}^{-1}$, the recovered symbol in (26) becomes

$$\begin{aligned} x' &= \boldsymbol{\Omega}^H y' \\ &= x + w'. \end{aligned} \tag{27}$$

where $\boldsymbol{w}'$ is the noise vector.

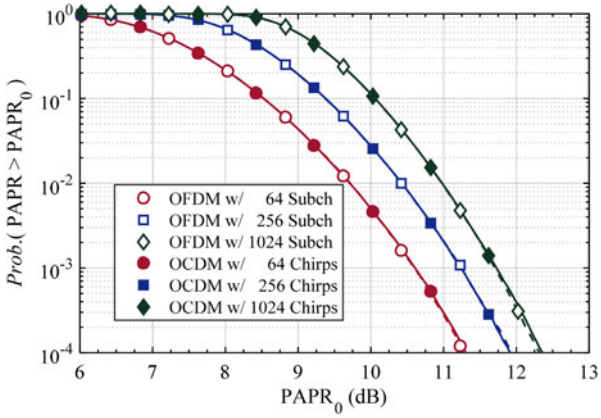

Fig. 5. PAPR performance of the OCDM and OFDM systems with various number of subcarriers and chirps.

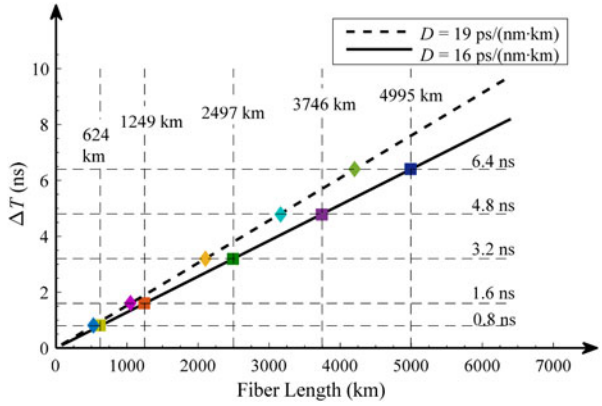

Fig. 6. Pulse broadening ΔT along with the transmission distance of SMF of different dispersion parameters.

IV. Analysis and Simulation Results

In this section, numerical simulations are carried out to validate the feasibility of the proposed CO-OCDM system and to investigate its transmission performance over SMF channel.

In the simulations, CO-OFDM is considered for comparison. In the OFDM/OCDM, there are 1024 subcarriers/chirps, which are modulated in quadrature amplitude modulation (QAM). In the CO-OCDM system, receiver #2 is adopted for its efficiency. Channel estimation is achieved by the frequency-domain pilot designed for the CO-OFDM system [30], and it is also adopted for the proposed CO-OCDM system.

The system setup is based on Fig. 4. The sampling rate of the D/A and A/D convertors is at 10 GS/s. Thus, the data rate is 20 Gbit/s for 4-QAM or 40 Gbit/s for 16-QAM. In the simulation, from the digital-to-analog process, raised cosine filter of a roll off factor 0.05 is employed to emulate the bandlimited signal with an oversampling ratio of 8. The wavelength is at 1550 nm; the IQ modulator is operated within linear region. At the receiver, the responsivity of PDs is 1 A/W. The coherent receiver converts the optical signal into the electrical baseband signal.

The optical link consists of 80-km SMF loops, and each loop is followed by an optical amplifier. The SMF has a dispersion $D = 16\ \mathrm{ps/(km \cdot nm)}$ and loss $0.2\ \mathrm{dB/km}$. The nonlinear Kerr effect in the fiber is considered with a nonlinear coefficient $2.6 \times 10^{-20}\ \mathrm{m^2/W}$. It is simulated by split-step Fourier method. After every 80-km transmission, an optical amplifier with a gain of 16 dB compensates the power loss of the signal.

A. Peak-to-Average Power Ratio

In this subsection, the PAPR characteristics of the proposed CO-OCDM system is studied. In the CO-OCDM system, there are 64, 256, and 1024 chirps with 16-QAM. Similarly, there are 64, 256, and 1024 subcarriers in the CO-OFDM system. The baseband signal is oversampled by a factor of 4 to simulate the actual PAPR which is evaluated by complementary cumulative distribution function (CCDF).

In Fig. 5, the CCDFs of the PAPR are provided. It is shown that, in the same condition, the OFDM and OCDM get the same PAPR performance. This can be inferred from the mechanism of OFDM and OCDM systems. In the OFDM, subcarriers are combined while in the OCDM chirps are combined in the same way. From the view of formulation in (12), the OCDM signal introduces only chirped phase shift on OFDM signal.

Observing the system structure of OCDM and OFDM in Fig. 2, the OCDM is also a 'multicarrier' system, which employs the orthogonal chirps as subcarriers for modulation. One can easily inter that the PAPR reduction methods, which are designed for OFDM systems [31], can be also adapted for the proposed CO-OCDM system for PAPR improvement.

B. Chromatic Dispersion

Chromatic dispersion is the major dispersion effect in SMF, causing pulse broadening. If the bandwidth of the optical signal is B, the pulse broadening after SMF transmission is

$$\Delta T = \beta_2 L B, \tag{28}$$

where β_2 is the group velocity dispersion (GVD) parameter, L is defined as the length of the fiber. Usually, the dispersion is measured by the dispersion parameter D, which has units of ps/(km · nm). It is defined as

$$D = -\frac{2\pi}{\lambda^2} c \beta_2, \tag{29}$$

where c is the speed of light and λ is the operating wavelength. In practice, the dispersion parameter D of the standard SMF is usually from 16 to 23 ps/(km · nm).

Fig. 6 illustrates the pulse broadening against transmission distance. It can be observed that the pulse broadening increases linearly along with the transmission distance L and the dispersion parameter D. For example, for a dispersion parameter $D = 16\ \mathrm{ps/(km \cdot nm)}$, a 4995-km SMF transmission will cause a $\Delta T = 6.4\,\mathrm{ns}$ pulse broadening. If D increases to 19 ps/(km · nm), the distance decreases to 4400 km.

In Fig. 7, the performance of CO-OCDM with various GI lengths is evaluated at different transmission distance in terms of average Q factor. In the simulation, to manifest the impact of

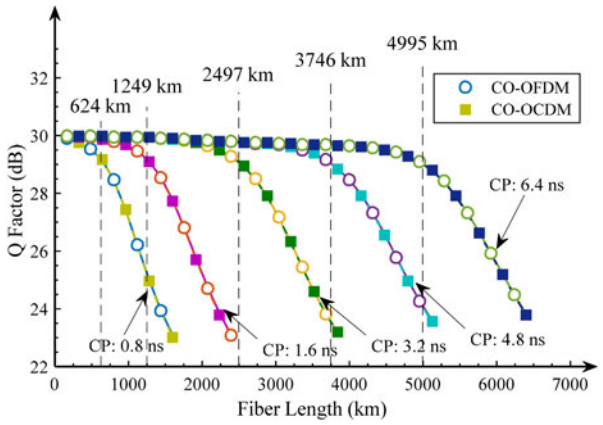

Fig. 7. Average Q factor versus transmission distance of the CO-OCDM and CO-OFDM systems with different guard interval (GI) length.

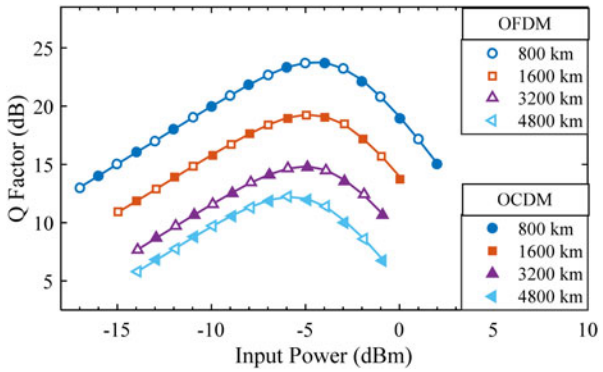

Fig. 8. Average Q factors versus input powers of CO-OFDM and CO-OCDM systems at various SMF transmission with 6.4-ns GI.

chromatic dispersion, both the nonlinear effect and inline ASE noise were not included. The noise is added at the receiver at a fixed $\mathrm{SNR} = 30$ dB. It can be observed that both systems get no obvious degradation as long as the GI length is longer than the pulse broadening. For example, if the GI length $= 0.8$, 1.6, 3.2, 4.8, or 6.4 ns, the performance starts to degrade if the distance exceeds 624, 1249, 2497, 3746, or 4995 km.

In Fig. 7, both the CO-OFDM and CO-OCDM have the same averaged Q factors for the same condition. We will show later that though the averaged Q factors of both systems are the same, the CO-OCDM system is more resilient to channel impairments due to the spectral fading and noise effects of a communication system. As a result, the CO-OCDM system exhibits better BER performance than the CO-OFDM.

C. Nonlinear Effects

Fiber nonlinearity imposes limitation on the reach of optical systems. In Fig. 8, we investigate the effect of fiber nonlinearity on the performance of CO-OCDM. The length of GI is 6.4 ns to support a transmission up to 5000-km. In the simulation, in-line ASE noise is introduced by the EDFA with a noise figure of 4.6 after every 80-km SMF transmission. The performance is also evaluated by the average Q factor with various input power.

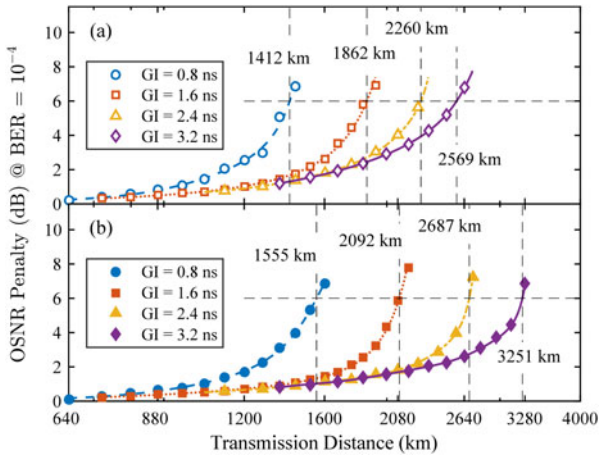

Fig. 9. OSNR penalties of (a) CO-OFDM and (b) CO-OCDM systems of 16-QAM to achieve a $\mathrm{BER} = 10^{-4}$ at different transmission distance.

In Fig. 8, as the transmission distance increases from 800 km to 5600 km, the optimal input power varies from -4.5 to -6 dBm. The similar nonlinear tolerances of both the OCDM and OFDM systems can be inferred from that they have the same PAPR characteristics, as shown in Fig. 5.

D. OSNR Penalty Versus Transmission Distance at Fixed BER

In Fig. 9, we evaluate the OSNR penalties to achieve a $\mathrm{BER} = 10^{-4}$ at different transmission distances. The input power is fixed at -5 dBm, and no inline noise is considered. The OSNR with 0.1-nm resolution (12.5 GHz at 1550 nm) is measured at the receiver in single polarization. The GI varies from 0.8 to 3.2 ns.

The CO-OCDM system outperforms the CO-OFDM system if the length of GI is the same, though both systems get almost the same average Q-factor as indicated in Figs. 7 and 8. At an OSNR penalty of 6 dB, the CO-OCDM improves transmission distance by 10.1%, 12.4%, 18.9%, and 26.5% compared to the CO-OFDM for GI $= 0.8$, 1.6, 2.4, and 3.2 ns, respectively.

The improvement achieved by OCDM is because it is more resilient to channel impairments than OFDM. In the next subsection, we will investigate the reason of this improvement by measuring the channel frequency responses of both systems. Experiments in Section V also confirm the simulation results.

E. BER Performance of Various Modulation Levels

In this subsection, we investigate the BER performance of the CO-OCDM systems with various modulation levels. The GI is chosen to be 1.6-ns and 3.2-ns long to support the transmission up to 1200-km and 2400-km, respectively.

In Fig. 10(a), the length of GI is 1.6 ns while in Fig. 10(b), it is 3.2 ns. In the 4-QAM case, the OSNR penalties at 1200-km are 2 dB for 1.6-ns GI and 1 dB for 3.2-ns GI at a $\mathrm{BER} = 10^{-6}$. If 16-QAM is adopted, the penalties become about 3.5 dB and 2 dB, respectively. In both cases, the CO-OCDM achieves better BER performance than the CO-OFDM.

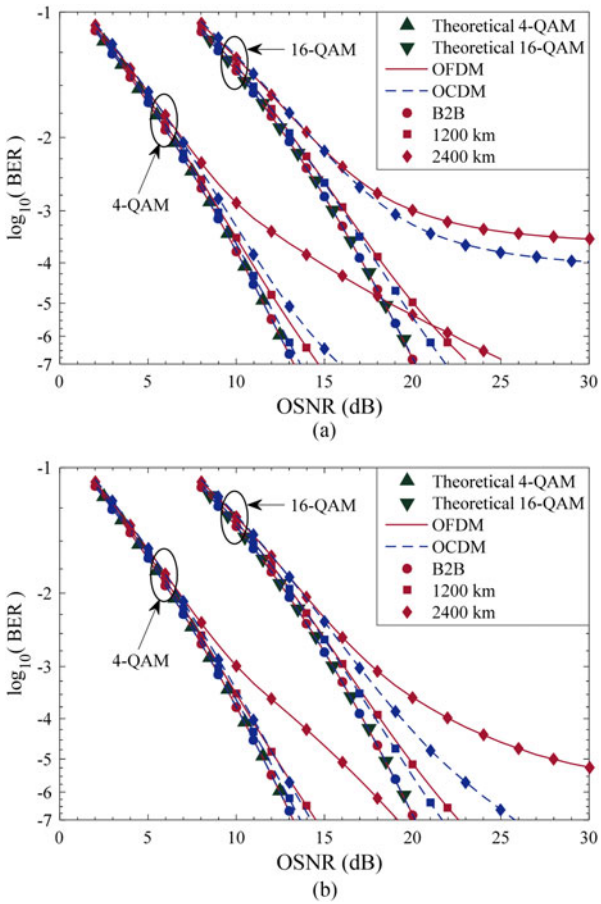

Fig. 10. BER versus OSNR performance of the CO-OFDM/OCDM systems with (a) 1.6-ns and (b) 3.2-ns GI.

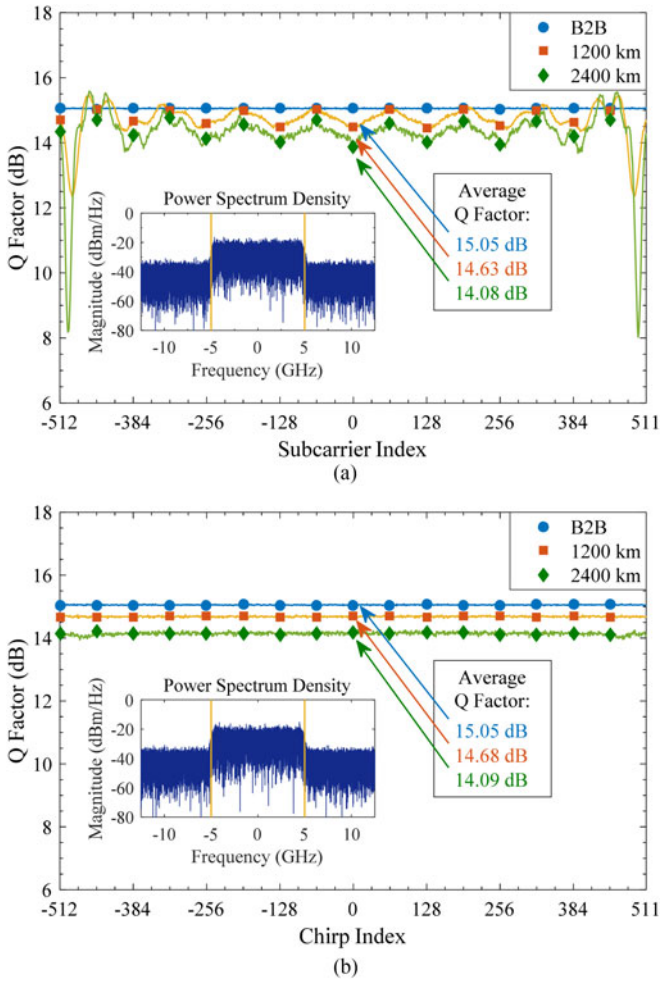

Fig. 11. Q factor of each (a) subcarrier in the CO-OFDM or each (b) chirp in the CO-OCDM with 3.2-ns GI at a received OSNR = 15 dB.

As the transmission distance increases to 2400 km, the BER performance penalty, especially for the 16-QAM case, becomes pronounced. In the case of 16-QAM with GI $= 1.6$ ns, there are even error floors in both systems because high level modulation scheme is more sensitive to the impairments due to insufficient GI. If GI increases to 3.2 ns, the error floor is alleviated. Still, in all cases of 2400-km transmission, the CO-OCDM system gets better performance than the CO-OFDM. For example, if GI $= 3.2$ ns, the CO-OFDM system needs additional 2-dB and 3-dB OSNR for 4-QAM and 16-QAM, respectively, to get a $\mathrm{BER} = 10^{-4}$ compared to the CO-OCDM.

To investigate the BER performance differences between the CO-OFDM and CO-OCDM, Fig. 11 provides the measured Q factors of (a) each subcarrier in CO-OFDM and (b) each chirp in CO-OCDM at a $\mathrm{OSNR} = 15\ \mathrm{dB}$. The Q factor is measured over 1×10^5 OFDM symbols by calculating the average signal variance. It can be observed that both systems have the same average Q factors at the same distance. However, the Q factors of the subcarriers in OFDM fluctuates; higher the frequency is, lower the Q becomes. The degradation becomes more severe as the distance increases.

In the simulation, the fading impairment is due to the edge effect, and it is explained as follows. In the OFDM, as well as the OCDM system, the aliasing signal at the edge of spectra after resampling (A/D conversion) will be out-of-phase due to the chromatic dispersion. After resampling the OFDM/OCDM signals at Nyquist rate for channel equalization and detection, the out-of-phase aliasing signal in the frequency domain causes the fading effect at the edge of the spectra. Therefore, the BER performance of OFDM system is limited by the noisy subcarriers at high frequency region.

On the other hand, in the CO-OCDM system, despite the uneven spectra, the Q factors of all the chirps are the same as the chirps spread their spectra over the entire bandwidth. As a result, the CO-OCDM system is insensitive to the fading effect.

V. Experiments

We implemented experiments to investigate the performance of the CO-OCDM system. At the transmitter, the OCDM signal is fed into an arbitrary waveform generator (AWG) with digital-to-analog (D/A) converters at 12 GS/s. There are 768 chirps which are modulated in 4-QAM and 16-QAM. To separate the aliasing signal, a pulse-shaping filter with up-sampling rate of 4/3 is adopted. Therefore, the bandwidth of the OCDM signal is 9 GHz, and the data rates are 18 Gbit/s for 4-QAM or

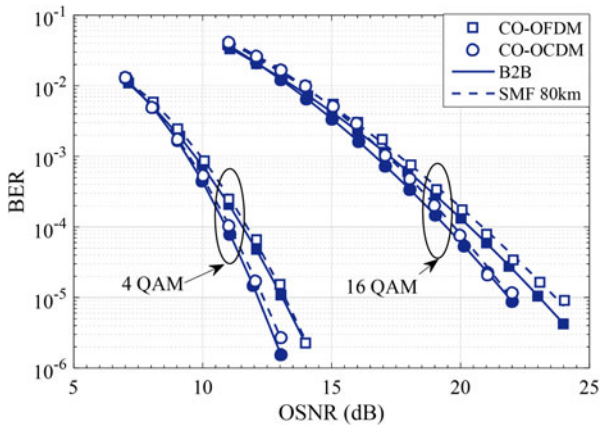

Fig. 12. Experiments results of the BER versus OSNR of the CO-OFDM and CO-OCDM systems.

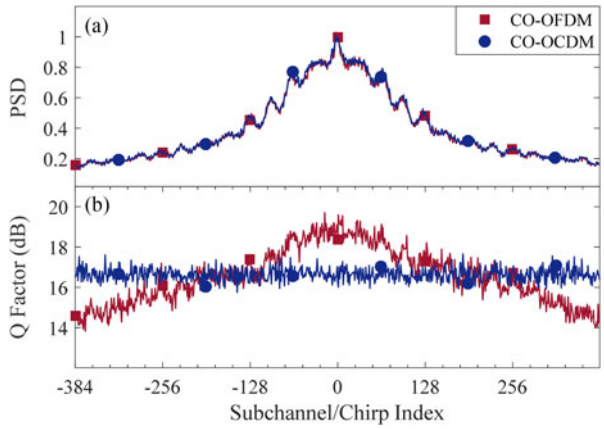

Fig. 13. The measured (a) power spectral densities (PSDs) and (b) Q-factors of each subchannel/chirp in the CO-OFDM and CO-OCDM systems.

36 Gbit/s for 16-QAM. In the OFDM system, 256 out of the 1024 subcarriers are also set to be zeros to achieve an oversampling rate of 4/3. Thus, the data rates of both systems are the same. The length of CP is 32 points. In the experiment, frequency-domain pilot for OFDM [30] is employed for channel estimation, as we used in the simulation. The Schmidl-Cox algorithm proposed in the OFDM system [32] is adopted for symbol synchronization for the CO-OCDM system. The electrical output of the AWG is amplified to drive the optical IQ modulator that is operated in linear region. The operating wavelength of the laser is 1553 nm.

After 80-km SMF transmission, the fiber loss is compensated by an EDFA, following by a 0.8-nm OBPF to remove the out-of-band ASE noise. An optical coherent receiver perceives the optical signal and converts the optical signal back to the electrical baseband signal. A real-time digital phosphor oscilloscope with 50-GS/s analog-to-digital (A/D) converters sample and store the baseband signal for offline processing. In the offline processing, after resampling and synchronization, the information bits are recovered based on Fig. 4.

In Fig. 12, the measured BER performance of CO-OFDM and CO-OCDM systems are shown. In the low OSNR region, both systems get similar performance. As the OSNR increases, the CO-OCDM requires lower OSNR than the CO-OFDM to achieve the same BER. For example, to reach a $\mathrm{BER} = 10^{-5}$, the CO-OCDM system requires about 1 dB OSNR less than the CO-OFDM system.

To investigate the performance difference, the measured (a) power spectral density (PSD) and (b) Q-factor of subchannels in OFDM or chirps in OCDM are provided in Fig. 13. It can be observed that both systems have the same PSD's and the same channel frequency responses, and the same average Q-factors. In the experiments, the uneven spectra are mainly caused by the electronic and optical devices, whose frequency responses are not ideally flat. That is, high frequency components experience severe fading effects. As a result, BER performances similar to those in the simulation can be observed in the experiments. In the CO-OFDM, the subcarriers of high frequency are noisier, and its BER performance is limited. In contrast, in Fig. 13(b), the chirps in the OCDM experience almost the same Q factors and are insensitive to the fading effect.

TABLE I
ARITHMETIC COMPLEXITIES OF THE CO-OFDM AND CO-OCDM SYSTEMS

Schemes			Number of complex multiplications
CO-OCDM	Receiver #1	TDE	$N\log_2 N + (4+L)N$
		FDE	$2N\log_2 N + 5N$
	Receiver #2		$1.5N\log_2 N + 3N$
CO-OFDM			$N\log_2 N + N$

N is the number of subcarriers/chirps in CO-OFDM/OCDM, and L is the number of taps in the transverse filter in TDE.

VI. DISCUSSIONS

A. Complexities of the CO-OCDM System

In this section, we will evaluate the arithmetic complexity of the CO-OCDM system in terms of complex multiplications. In the CO-OFDM/OCDM system, it is assumed that there are N subcarriers/chirps. In Fig. 4, excluding the components in the dashed-line boxes, the transmitter and receiver #2 constitutes a conventional CO-OFDM system.

In the CO-OFDM system, the transceiver has an IDFT and a DFT, whose complexity is $N\log_2 N$, and a single-tap equalizer, whose complexity is N. Therefore, the CO-OFDM system has a total complexity of $N\log_2 N + N$.

In the CO-OCDM system, the transmitter has an IDFnT with a complexity of $0.5\ N\log_2\ N + 2N$. In the receiver #1, there is one DFnT. If the transverse filter in TDE has L taps, its complexity is LN. In the FDE scheme in Fig. 4(b), there is a DFT, an IDFT, and single-tap equalizers, with a complexity of $N\log_2 N + N$. Thus, the CO-OCDM system with receiver #1 has a complexity of $N\log_2 N + (4+L)N$ for TDE or $2N\log_2 N + 5N$ for FDE.

On the other hand, the receiver #2 has a DFT, an IDFT and a single-tap equalizer and the phase cancellation operation due to Γ. As a result, the CO-OCDM system with receiver #2 has a total complexity of $1.5N\log_2\ N + 3N$.

In Table I, the arithmetic complexities of the CO-OFDM and the CO-OCDM are provided. In the receiver #1 with TDE, L is usually large if the dispersion of the channel is severe, and thus the complexity of the receiver #1 with TDE is higher than

the other schemes. The complexity of the receiver #2 is lower than that of the receiver #1 with either TDE or FDE, and it gets additional $0.5N\log_2 N + 2N$ to that of the CO-OFDM system.

It should be noted that there are other compulsory functional modules required for a communication system, such as clock recovery, timing and frequency synchronization. Although they have not been indicated in Fig. 4, they are crucial for a communication system. We will not consider their complexity since they need more detailed consideration.

B. Comparison to the Precoded OFDM

As illustrated in Fig. 2(b), the proposed CO-OCDM system synthesizes modulated orthogonal chirps for data transmission. It has intimate relations to but is different to OFDM, as well as the precoded OFDM with, such as, DFT, discrete trigonometric transforms, Walsh-Hadamard, and wrapped constant amplitude zero auto-correlation (CAZAC) matrices [33]–[36].

In the precoded OFDM, before DFT, symbols are precoded by a precoding matrix, and then multiplexed onto subcarriers for synthesis. In the digital implementation, it requires a matrix multiplication before the IDFT, though fast algorithms can be applied to some precoding matrices. The precoded OFDM may achieve improved performance, such as better PAPR characteristics and/or better BER transmission performance.

In the proposed CO-OCDM system, it is obvious that chirps are modulated directly by the DFnT. The CO-OCDM system is more resilient against the channel impairments than CO-OFDM and gets the same PAPR performance as CO-OFDM. Similar to OFDM, one can heuristically implement precoding process for the OCDM systems with various precoding matrices. In addition, different precoding matrices would exhibit various characteristics and performance for the OCDM system.

VII. Conclusion

In this paper, we have proposed the OCDM for optical fiber communication. DFnT implements the CO-OCDM system in the digital domain. Analysis and simulation are carried out to investigate the performance of the CO-OCDM signal in optical fibers. Experiment of 36-Gbit/s OCDM signal over 80-km SMF transmission are implemented to verify the feasibility of the proposed CO-OCDM system.

In virtue of chirp spread spectrum, the proposed CO-OCDM is more resilient to channel impairments and gets better BER performance than the CO-OFDM system. It can also be easily integrated into the existing CO-OFDM system with only slight modification. Therefore, based on the widespread CO-OFDM systems, the proposed CO-OCDM can be implemented as an alternative approach, which is more resilient to the channel impairments, to achieve high-speed optical communication.

References

[1] S. J. Savory, "Digital filters for coherent optical receivers," *Opt. Express*, vol. 16, no. 2, pp. 804–817, Jan. 2008.

[2] X. Li *et al.*, "Electronic post-compensation of WDM transmission impairments using coherent detection and digital signal processing," *Opt. Express*, vol. 16, no. 2, pp. 880–888, Jan. 2008.

[3] E. Ip, and J. M. Kahn, "Compensation of dispersion and nonlinear impairments using digital backpropagation," *J. Lightw. Technol.*, vol. 26, no. 17–20, pp. 3416–3425, Sep./Oct. 2008.

[4] P. J. Winzer and R. J. Essiambre, "Advanced optical modulation formats," *Proc. IEEE*, vol. 94, no. 5, pp. 952–985, May 2006.

[5] Y. Koizumi *et al.*, "1024 QAM (60 Gbit/s) single-carrier coherent optical transmission over 150 km," *Opt. Express*, vol. 20, no. 11, pp. 12508–12514, May 2012.

[6] Y. Han and G. F. Li, "Coherent optical communication using polarization multiple-input-multiple-output," *Opt. Express*, vol. 13, no. 19, pp. 7527–7534, Sep. 2005.

[7] H. Bulow, F. Buchali, and A. Klekamp, "Electronic dispersion compensation," *J. Lightw. Technol.*, vol. 26, no. 1–4, pp. 158–167, Jan/Feb. 2008.

[8] A. C. Singer, N. R. Shanbhag, and H. M. Bae, "Electronic Dispersion Compensation An overview of optical communications systems," *IEEE Signal Process. Mag.*, vol. 25, no. 6, pp. 110–130, Nov. 2008.

[9] S. J. Savory *et al.*, "Electronic compensation of chromatic dispersion using a digital coherent receiver," *Opt. Express*, vol. 15, no. 5, pp. 2120–2126, Mar. 2007.

[10] A. J. Lowery, and L. B. Du, "Optical orthogonal division multiplexing for long haul optical communications: A review of the first five years," *Opt. Fiber Technol.*, vol. 17, no. 5, pp. 421–438, Oct, 2011.

[11] W. Shieh, X. Yi, and Y. Tang, "Transmission experiment of multi-gigabit coherent optical OFDM systems over 1000 km SSMF fibre," *Electron. Lett.*, vol. 43, no. 3, pp. 183–185, Feb. 2007.

[12] B. J. C. Schmidt, A. J. Lowery, and J. Armstrong, "Experimental demonstrations of electronic dispersion compensation for long-haul transmission using direct-detection optical OFDM," *J. Lightw. Technol.*, vol. 26, no. 1–4, pp. 196–203, Jan./Feb. 2008.

[13] X. Ouyang, and J. Zhao, "Orthogonal chirp division multiplexing," to appear in *IEEE Trans. Commun.*, doi: 10.1109/TCOMM.2016.2594792, arXiv:1601.06576, 2016.

[14] X. Ouyang *et al.*, "Discrete Fresnel transform and its circular convolution," arXiv:1510.00574, 2015.

[15] H. F. Talbot, "Facts relating to optical science. No. IV," *Philosoph. Mag. Series 3*, vol. 9, no. 56, pp. 401–407, Dec. 1836.

[16] L. Rayleigh, "On copying diffraction-gratings, and on some phenomena connected therewith," *Philosoph. Mag. Series 5*, vol. 11, no. 67, pp. 196–205, Mar. 1881.

[17] J. T. Winthrop, and C. R. Worthing, "Theory of Fresnel images I. plane periodic objects in monochromatic light," *J. Opt. Soc. Amer.*, vol. 55, no. 4, pp. 373–381, 1965.

[18] J. M. Wen, Y. Zhang, and M. Xiao, "The Talbot effect: recent advances in classical optics, nonlinear optics, and quantum optics," *Adv. Opt. Photon.*, vol. 5, no. 1, pp. 83–130, Mar. 2013.

[19] F. Gori, "Why is the Fresnel transform so little known?," *Current Trends in Optics, Lasers and Optical Engineering*, J. C. Dainty, Ed.: New York, NY, USA: Academic, 1994, pp. 139–148.

[20] P. Szwaykowski, and V. Arrizon, "Talbot array illuminator with multilevel phase gratings," *Appl. Opt.,* vol. 32, no. 7, pp. 1109–1114, Mar. 1993.

[21] V. Arrizon, and J. Ojeda-Castaneda, "Multilevel phase gratings for array illuminators," *Appl. Opt.,* vol. 33, no. 25, pp. 5925–5931, Sep. 1994.

[22] V. Arrizon, and J. Ojeda-Castaneda, "Fresnel diffraction of substructured gratings: Matrix description," *Opt. Lett.*, vol. 20, no. 2, pp. 118–120, Jan. 1995.

[23] V. Arrizon, J. G. Ibarra, and J. OjedaCastaneda, "Matrix formulation of the Fresnel transform of complex transmittance gratings," *J. Opt. Soc. Amer. A*, vol. 13, no. 12, pp. 2414–2422, Dec. 1996.

[24] C. H. Zhou, and L. R. Liu, "Simple equations for the calculation of a multilevel phase grating for Talbot array illumination," *Opt. Commun.*, vol. 115, no. 1/2, pp. 40–44, Mar. 1995.

[25] S. B. Weinstein, and P. Ebert, "Data transmission by frequency-division multiplexing using discrete Fourier transform," *IEEE Trans. Commun. Tech.*, vol. CT-19, no. 5, pp. 628–634, Oct. 1971.

[26] S. Darlington, "Demodulation of wideband low-power FM signals," *Bell Syst. Tech. J.*, vol. 43, no. 1, pp. 339–374, 1964.

[27] A. Kadri, R. K. Rao, and J. Jiang, "Low-power chirp spread spectrum signals for wireless communication within nuclear power plants," *Nuclear Technol.*, vol. 166, no. 2, pp. 156–169, May 2009.

[28] M. Palmese *et al.*, "Experimental validation of a chirp-based underwater acoustic communication method," in *Proc.7th Eur. Conf. Noise Control June 29, 2008–July 4, 2008*, Paris, France, 2008, pp. 147–152.

[29] J. Proakis, and M. Salehi, *Digital Communications*, 5th ed. New York, NY, USA: McGraw-Hill Edu., 2007.

[30] Y. S. Liu, Z. H. Tan, H. J. Hu, L. J. Cimini, G. Y. Li, "Channel estimation for OFDM," *IEEE Commun. Surveys Tuts.*, vol. 16, no. 4, pp. 1891–1908, May 2014.
[31] S. H. Han, and J. H. Lee, "An overview of peak-to-average power ratio reduction techniques for multicarrier transmission," *IEEE Wirel. Commun.*, vol. 12, no. 2, pp. 56–65, Apr. 2005.
[32] T. M. Schmidl, and D. C. Cox, "Robust frequency and timing synchronization for OFDM," *IEEE Trans. Commun.*, vol. 45, no. 12, pp. 1613–1621, Dec. 1997.
[33] M. Sung, S. Kang, J. Shim, J. Lee, and J. Jeong, "DFT-precoded coherent optical OFDM with Hermitian symmetry for fiber nonlinearity mitigation," *J. Lightw. Technol.*, vol. 30, no. 17, pp. 2757–2763, Sep. 2012.
[34] M. Sung, J. Lee, and J. Jeong, "DCT-precoding technique in optical fast OFDM for mitigating fiber nonlinearity," *IEEE Photon. Technol. Lett.*, vol. 25, no. 22, pp. 2209–2212, Nov. 2013.
[35] Z. Feng *et al.*, "Dispersion-tolerant DDO-OFDM system and simplified adaptive modulation scheme using CAZAC precoding," *J. Lightw. Technol.*, vol. 34, no. 11, pp. 2743–2751, Jun. 2016.
[36] Z. H. Feng *et al.,* "Performance-enhanced direct detection optical OFDM transmission with CAZAC equalization," *IEEE Photon. Technol. Lett.*, vol. 27, no. 14, pp. 1507–1510, Jul. 2015.

Xing Ouyang received the M.S. degree in information science and engineering from Dalian Polytechnic University, China, in 2013. He is currently with Tyndall National Institute, Cork, Ireland, and also with the School of Electrical and Electronic Engineering, University College Cork, Cork, Ireland. His current research interests include multicarrier transmission techniques and digital signal processing in both the wireless and optical communication systems, as well as the transmitter and receiver diversity techniques for fading communication channels.

Jian Zhao received the B.Eng. degree from the University of Science and Technology of China, Hefei, China, in 2002, and the M.Phil. and Ph.D. degrees from the Chinese University of Hong Kong, Hong Kong, in 2004 and 2007, respectively. He is currently with Tyndall National Institute, Cork, Ireland, University College Cork, Cork, Ireland. Since 2009, he has received more than €2.4 million funding as the Principal Investigator from Science Foundation Ireland, EU FP7, Industry, Enterprise Ireland, and Irish Research Council. He is also the Co-PI of two Hong Kong Research Grant Council projects. He holds two patents and has published more than 110 technical papers (more than 75 senior-author papers and 16 invited papers) in peer-reviewed international journals and conference proceedings. His current research interests include optical OFDM, advanced modulation and detection schemes, digital signal processing for optical communications, and fiber nonlinearity mitigation. He received the SFI Career Development Award in 2016, the Starting Investigator Research Award in 2012, and the Technology Innovation and Development Award in 2013. The team he led was the EMEA finalist in Alcatel-Lucent Innovation Competition in 2012. He has served as a TPC Member/Co-Chair in more than 10 conferences, and is a Reviewer for Funding for Scientific Research Belgium, Hong Kong Research Grants Council, and various journals including *Optics Express*, *Optics Letters*, the *Journal of Lightwave Technology*, *Photonics Technology Letters*, the *Journal of Optical Communications and Networking*, IEEE TRANSACTIONS ON VEHICULAR TECHNOLOGY, and so on.